Growth of Polar Hexagonal Boron Nitride Monolayer on Nonpolar Copper with Unique Orientation

Jidong Li, Yao Li, Jun Yin, Xibiao Ren, Xiaofei Liu, Chuanhong Jin, and Wanlin Guo*

Hexagonal boron nitride (h-BN), a layered III–V insulator with a wide band gap, is of honeycomb lattice similar to that of graphene but composed of alternating boron and nitrogen atoms instead of all carbon atoms. The strong ionicity of B–N bonds endows h-BN with ultrahigh in-plane mechanical strength,[1] supreme thermal stability up to 1000 °C, and chemical inertness.[2] These outstanding properties of h-BN have stimulated a wide range of applications from protective coatings to ultraviolet emitters.[3,4] More recently, when being hybridized with other 2D materials, h-BN has exhibited remarkable performance serving as substrates and ultrathin tunneling dielectric.[5,6] Its atomically smooth and chemically inert surface makes it an ideal substrate for probing the intrinsic and stable performance of graphene, transitional metal dichalcogenides, and black phosphorus.[7,8] With h-BN sandwiched between two graphene layers, extraordinary device performance and new physical phenomenon have been explored.[6,9] Deep insights into the interactions between h-BN and the neighboring layers prove that the electrical performances of these devices could be significantly dependent on the relative lattice orientation between the neighboring layers. For instance, the Hofstadter's butterfly, commensurate-incommensurate state and tunneling behavior in the stacked graphene/h-BN structure are closely related to the stacking orientation.[10,11] In order to fabricate devices with expected performance, preparation of h-BN with unique lattice orientation is requested.

Chemical vapor deposition (CVD) has been successfully employed to synthesize h-BN monolayer in large area.[12–14] However, the orientations of the CVD h-BN crystal domains are generally in random distribution, and the resultant grain boundaries would severely reduce the chemical inertness of h-BN and arouse localized boundary states.[13,15] To address this issue, a lot of efforts have been made to suppress the predominant orientations through van der Waals (vdW) epitaxy on various noble single crystals, including Pt(111), Ni(111), and Ge(110).[13,16,17] It is expected that unidirectionally aligned h-BN nuclei can grow and then coalesce into a single crystal without grain boundaries,[18] similar to the case of graphene.[19,20] However, the h-BN nuclei frequently take at least two opposite predominant orientations due to the polar structure of h-BN. This case is analogous to the well-known antiphase phenomenon in conventional polar-on-nonpolar epitaxy[21] and also happens for other polar 2D materials, such as MoS_2 and Bi_2Se_3.[22,23] Although the antiphase disorder in conventional polar-on-nonpolar epitaxy of GaAs can be suppressed through step doubling on Si(100) surface or using Si(211) surface as substrate,[21] these methods cannot be applied to the vdW epitaxy of 2D materials, because the relative orientation between the epitaxial 2D layer and substrate is determined by vdW interaction instead of covalent bonds. The solution for this problem is not clear, until very recently a method of dosing borazine at room temperature with following high temperature annealing has been developed for the growth of h-BN on Ir(111).[24] However, this sophisticated method is limited by the noble Ir substrate, and the h-BN domain size is only around 90 nm.

Here we demonstrate that h-BN triangular domains grown on Cu(102) or Cu(103) through low pressure CVD share a unique lattice orientation. One of their zigzag edges are aligned perpendicular to the symmetry axis of the Cu substrate, which according to our density functional theory calculations can be understood in terms of the minimization of vdW energy. This oriented configuration of the h-BN domains on Cu(102) and Cu(103) is in sharp contrast with that on widely studied Cu(111) and Cu(100).[25,26] Based on the preferred configuration of h-BN nucleus with respect to the symmetry axis of the substrate, we classify h-BN nuclei (the initially nucleated small triangle flakes) into three types, namely, antiphase, unidirection, and tiltedphase nucleus, covering all the cases observed by us and other groups. These results provide a viable strategy for growing h-BN monolayers with required orientations.

Low pressure CVD was conducted to grow monolayer h-BN on copper foil (see the Experimental Section for the detailed process). To elucidate the properties of obtained

J. Li, Y. Li, J. Yin, X. Liu, Prof. W. Guo
State Key Laboratory of Mechanics and Control
of Mechanical Structures
Key Laboratory for Intelligent Nano Materials
and Devices of the Ministry of Education
and Institute of Nanoscience
Nanjing University of Aeronautics and Astronautics
Nanjing 210016, China
E-mail: wlguo@nuaa.edu.cn

X. Ren, Prof. C. Jin
State Key Laboratory of Silicon Materials
School of Materials Science and Engineering
Zhejiang University
Hangzhou 310027, China
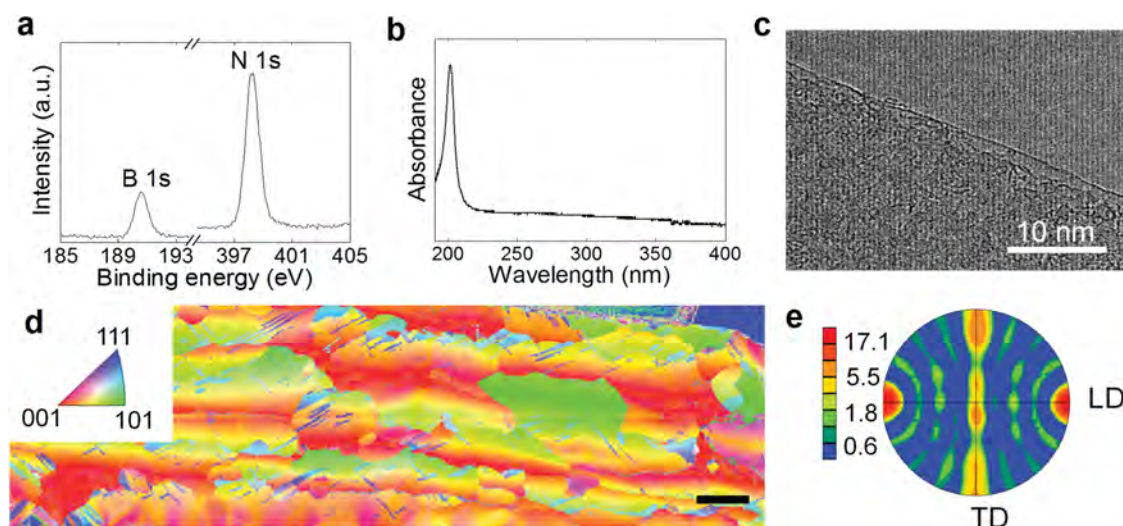
Figure 1. Characterization of h-BN and copper substrate. a) X-ray photoemission spectrum (XPS) of h-BN on Cu foil shows typical B1s and N1s peak. b) UV–vis spectrum of the h-BN transferred to quartz. c) Transmission electron microscopy (TEM) image shows an edge of h-BN monolayer. d) Electron back-scatter diffraction (EBSD) image of a copper foil surface. Scale bar is 1 mm. e) Corresponding {001} pole figures.

h-BN film, X-ray photoemission spectrum (XPS), and UV–vis spectrum were performed. As shown in **Figure 1**a, typical B1s and N1s peaks appear at 190.5 and 398.1 eV, respectively, verifying the B–N sp² bond. No obvious component peak around B1s and N1s core levels is observed, indicating that there is no covalent interaction between h-BN and the underlying Cu substrate. The UV–vis absorption spectrum of h-BN film transferred on quartz shows a sharp absorption peak around 202 nm (Figure 1b). The deduced optical band gap is 6.06 eV, which corresponds to that of monolayer h-BN. The single atomic layer of the h-BN film is further confirmed by the transmission electron microscopy (TEM) image taken at the edge of the film (Figure 1c). For the purpose of facilely characterizing crystalline h-BN domains, partially covered h-BN films were obtained by reducing the growth time. It is found that the h-BN domains are nearly perfect equilateral triangular in shape. Selected-area electron diffraction (SAED) pattern of one h-BN triangle indicates that it is single crystal with edges primarily along the zigzag orientation of the h-BN lattice (Figure S1, Supporting Information), which is consistent with previous results that h-BN triangles are prone to nitrogen-terminated zigzag edges.[27] Our previous work also demonstrated that nitrogen-terminated zigzag edges are the most stable configuration under electron beam irradiation.[28,29] The edges of the h-BN triangles exclusively illustrate the zigzag lattice orientation and thus provide a facile way to distinguish the lattice orientation of the epitaxial h-BN layers. For h-BN domains of irregular shapes, their crystalline orientations can be identified by optical second-harmonic generation.[30,31]

In order to probe the local crystal orientations of the underlying copper foil, electron back-scatter diffraction (EBSD) mapping was performed on copper foil after the growth of h-BN. Figure 1d shows the EBSD map of a copper foil that has grown h-BN domains. The corresponding {001} pole figure (Figure 1e) of the map demonstrates a <010> fiber texture of the copper foil, which means that most grains of the foil surface align their [010] directions parallel to the

longitudinal direction (LD, as marked in Figure S2, Supporting Information) of the foil strip. The exact orientations of crystal facets in local area, which may slightly vary from this statistical result, are further confirmed by the EBSD data for the following discussion.

In contrast to the common plate texture of annealed Cu foil (Figure S3, Supporting Information), the fiber texture observed here is probably attributed to the stress introduced into copper foil between the first and second annealing processes (see the Experimental Section for details). It is consistent with classical theory that face-centered cubic metal tends to be <010> or <111> fiber texture under drawing deformation.[32]

To reveal the orientation dependence of epitaxial h-BN on Cu substrate, we investigated h-BN triangles grown on different Cu facets, including Cu(111) on plate-textured Cu foil and a series Cu(x 0 y) facets on fiber-textured Cu foil. **Figure 2** shows the superimposed scanning electron microscope (SEM) images and corresponding EBSD maps of Cu substrates with (111), (102), and (103) facets. The h-BN triangles epitaxially grown on Cu(111) show two preferred orientations opposite to each other. This is consistent with previous reports[25] and analogous to the antiphase phenomenon in conventional polar-on-nonpolar epitaxy. In sharp contrast, on Cu(102) and (103), almost all of the epitaxial h-BN triangles are aligned along the same orientation, with one of their edges parallel to the [010] orientation. The few misaligned h-BN domains might be attributed to the disturbance arising from impurities on copper surface. The statistical distribution of the orientations of h-BN triangles in an area over 10^4 μm² (Figure S4, Supporting Information) are shown in Figure 2d. The misorientations within ±3° are ignored here, because the h-BN domains are not strictly equilateral triangles, which make it hard to determine the lattice orientation of h-BN with high precision. It can be found that over 97% h-BN triangles on Cu(102) or Cu(103) share the same orientation, and h-BN triangles of other orientations contributes less than 3%. On Cu(111), the
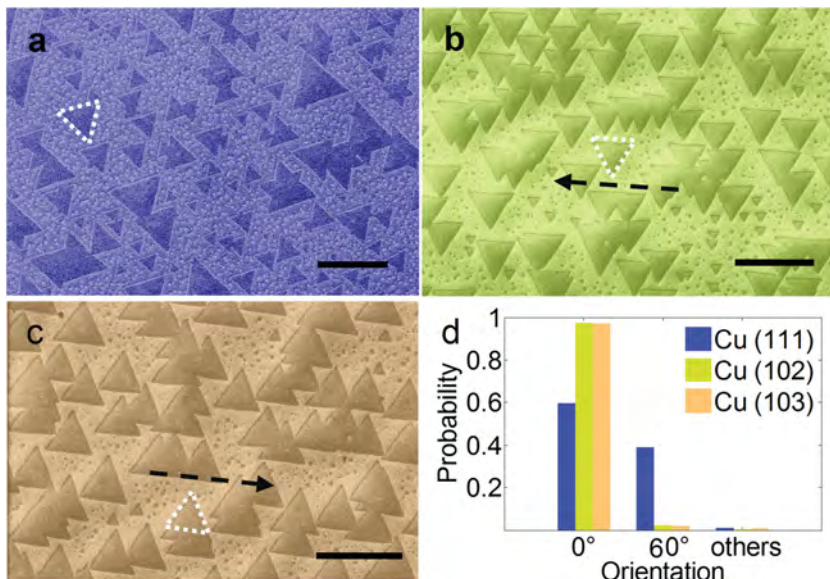
Figure 2. Aligned growth of h-BN domains on different Cu facets. a–c) Scanning electron microscope (SEM) images, superimposed with EBSD color, shows h-BN triangles grown on a) Cu(111), b) Cu(102), and c) Cu(103). Scalar bars in (a–c) are 20 μm. Black dashed arrows in (b) and (c) points Cu [010] direction with an angle error less than ±3°. White dashed triangles in (a–c) define the 0° orientation of the h-BN triangles on Cu(111), Cu(102), and Cu(103), respectively. d) Orientation statistics of the h-BN triangles grown on these three Cu facets.

numbers of h-BN triangles with opposite orientations are close to each other.

It is further showed that h-BN triangles with uni-orientation can be epitaxially grown not only on the exact Cu(102) and (103) facets but also on the Cu surfaces very close to these two facets. A careful examination of an area displayed in **Figure 3**a shows that h-BN triangles grown on Cu($\bar{3}$ 0 8) and Cu(7 0 12) are also of unique orientation, as illustrated in Figure 3b,c. It is the same for Cu(5 0 11) and Cu(5 0 9), as shown in Figure S5 in the Supporting Information. However, on some Cu(x 0 y) facets that deviate far from Cu(102) and Cu(103), h-BN triangles exhibit two predominant directions with a small included angle. The included angle is ≈10° for Cu(205), ≈16° for Cu(207) and ≈14° for Cu(105) (Figure 3c and Figure S6, Supporting Information). It should be noted that these two different orientations are of mirror symmetry relative to the symmetry axis of the Cu surface, as labeled in the inset of Figure 3c. In Figure 3b,d, there are also some crystalline microstrips with Cu(5 7 10), Cu(7$\bar{1}$0 13), and Cu($\bar{2}$ $\bar{5}$ 4) surfaces where h-BN triangles generally show two opposite orientations. However, we just focus on h-BN grown on Cu(x 0 y) facets here, further discussion of the situation observed on these microstrips are beyond the scope of this work.

It can be seen in Figure 3 that h-BN domains expanding across the Cu grain boundaries still keep in original shapes and orientations, instead of adapting to the new Cu grains. This indicates that the orientation of h-BN domain is determined and nailed down during the nucleation, then the domain will grow with the determined orientation.

To understand the mechanism of the unidirectional growth of h-BN on Cu(102) and Cu(103), we simulated a triangular h-BN nucleus with varying orientations on these

two facets as well as Cu(111) using density functional theory (DFT) calculations. The edges of h-BN nuclei in the models are hydrogen passivated. The corrugations of stacking energy with different stacking angles are shown in **Figure 4** where the stacking energy of 0° is set as zero point (see the configuration of 0° orientation in Figure S7, Supporting Information). It is found that the stacking energy reaches the minimum value at 60° for both Cu(102) and Cu(103) with energy barriers of ≈253.7 and ≈276.7 meV, respectively. And there is only one minimum energy in the 120° rotation period. However, there are two minimum values at 30° and 90° for Cu(111).

The energy differences between different orientations could be understood from vdW interaction between h-BN nuclei and Cu substrates. The average vertical distance between h-BN nucleus and underlying Cu(102) surface reduces from 2.746 to 2.640 Å as the orientation rotates from 0° to 60° (Figure S8, Supporting Information). This complies with the corrugations of stacking energy, since the vdW energy of two atoms of distance R is inversely proportional to R^6. It is similar for Cu(103) except relative large discrepancy between corrugations of the distance and stacking energy at some specific points. We attribute these variations to the structure buckling at these orientations.

The top view of the preferred orientations of h-BN nuclei on different Cu facets are shown in Figure 4b,e,h. It can be seen that at 60°, i.e., orientation with minimum energy, one zigzag edge of h-BN nucleus is exactly perpendicular to the symmetry axis of the substrate for Cu(102) and Cu(103). For Cu(111), although one zigzag edge of h-BN nucleus is also perpendicular to the symmetry axis of substrate surface, there are two preferred orientations opposite to each other and the stacking energies of these two antiphase states is very close. It is because that, compared with Cu(102) and Cu(103), the surface of Cu(111) is much more flat and the h-BN nucleus mainly interacts with the Cu atoms on the topmost layer of Cu(111). Besides the symmetry axis of (111) substrate, the topmost layer Cu is of mirror symmetry relative to [1$\bar{1}$0] orientation, giving rise to the similar stacking energy for the two opposite orientations. This kind of orientation is referred to as quasi-symmetry axis of Cu hereafter. Due to the larger lattice constant of the copper surface of facets such as Cu(205), and thus much higher computational cost, these cases are not simulated in our work, but it is observed that the two preferred tilted orientations are of mirror symmetry relative to the symmetry axis of the substrate.

The schematic illustration in **Figure 5** clearly describes three different epitaxial molds of h-BN with respect to the symmetry of Cu substrate: antiphase, unidirection, and tiltedphase. For antiphase epitaxy, h-BN nuclei of two opposite orientations are of mirror symmetry relative to either the
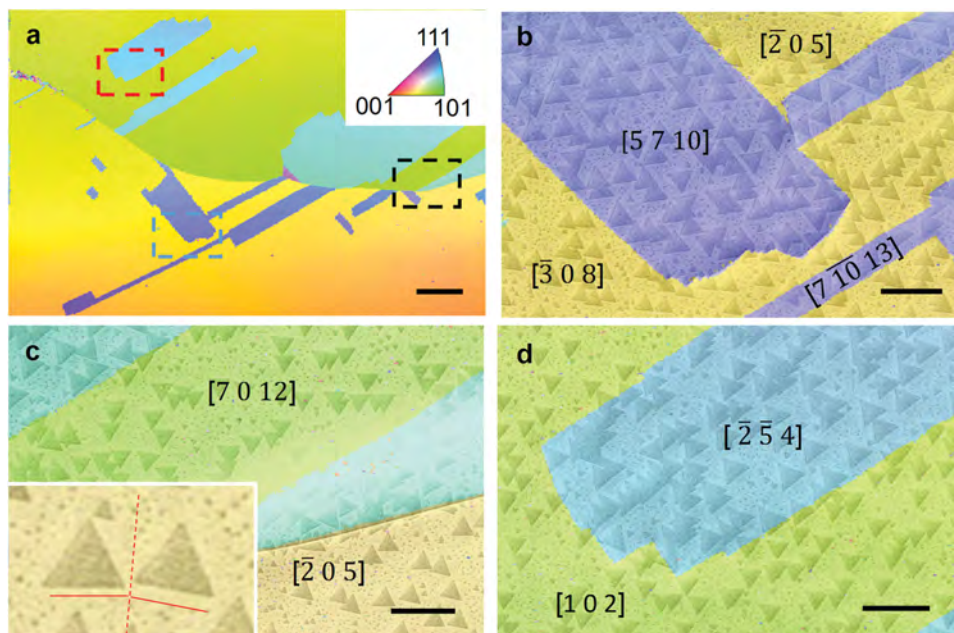
Figure 3. Magnified images of the copper foil with aligned h-BN domains. a) Magnified EBSD image of an area on the copper foil shown in Figure 1. Scalar bar is 100 μm. b–d) Superimposed SEM images and EBSD images in the area of blue, black and red rectangles in (a), respectively. Scalar bars are 20 μm. The inset of (c) is a magnified image of two h-BN triangles on Cu(205) with different orientations. The symmetry axis of Cu(205) is marked by a red dashed line and the orientations of the h-BN triangles are marked by red solid line.
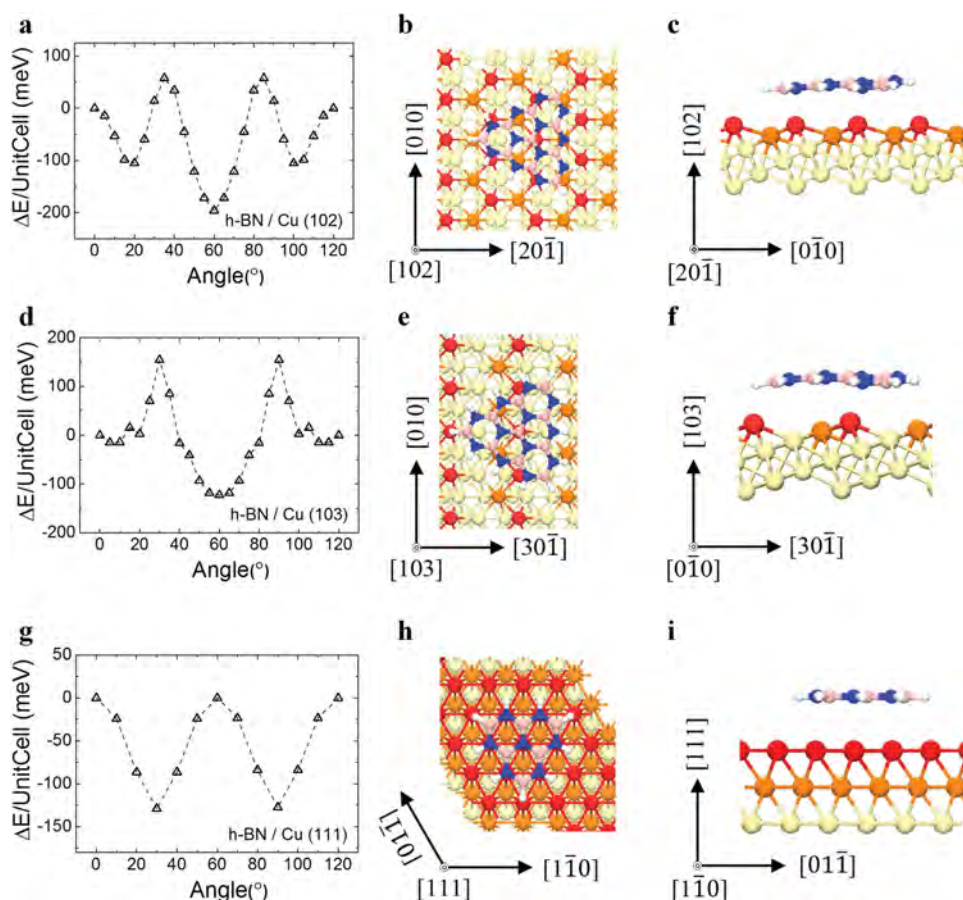
Figure 4. Orientation dependent stacking energies and the optimized structures based on DFT simulation. a,d,g) Energy corrugations of h-BN rotating on Cu(102), Cu(103), and Cu(111), respectively. The optimized 60° stacking structures are shown for h-BN on b,c) Cu(102), e,f) Cu(103), and 30° stacking structures for h-BN on h,i) Cu(111). Top view in b), e), and h). Side view in c), f), and i). Nitrogen in blue, boron in pink, and copper in yellow. Top and second atom layers of Cu facets are highlighted by red and orange colors, respectively.
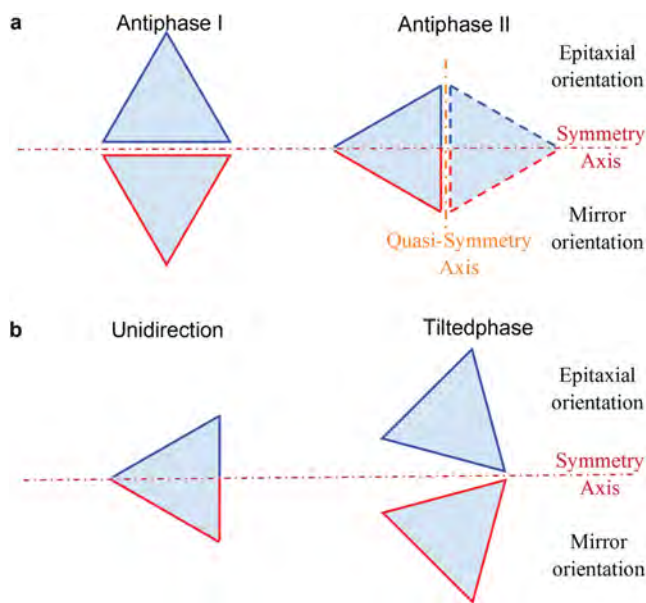
Figure 5. Classification of aligned van der Waals epitaxy. Schematic illustration of three types of aligned van der Waals epitaxy classified based on the relationship between the preferred epitaxial orientations and the symmetry axis of the substrate: a) antiphase state, b) unidirectional state, and tiltedphase state.

symmetry axis of the substrate (antiphase I) or the quasi-symmetry axis (antiphase II), as shown in Figure 5a. For antiphase I epitaxy, the stacking energy of these two preferred orientations should be exactly the same, as in the case of Cu(100).[25] For antiphase II epitaxy, the stacking energy of the two opposite orientations is unequal but very close, as in the case of Cu(111) discussed above. Notably, we observed unidirectional and tiltedphase epitaxy. To obtain unidirectional epitaxy, one edge of the triangle of the preferred epitaxial orientation is required to be perpendicular to the symmetry axis of the substrate, and the substrate is required to be of onefold or threefold symmetry without any quasi-symmetry axis, as shown in the case of Cu(102) and (103). For tiltedphase epitaxy, all edges of the triangular nucleus are neither perpendicular nor parallel to the symmetry axis, resulting in an oblique rotation angle between the two equivalent orientations, as shown in the case of Cu(205), Cu(207), and Cu(105).

In summary, we have demonstrated the vdW epitaxy of h-BN monolayer with unique orientation on Cu(102) and (103) during chemical vapor deposition. The unidirectional epitaxy is attributed to the onefold symmetry of these two facets without any quasi-symmetry axis and the parallel alignment of the symmetry axes of h-BN nucleus and the underlying Cu substrate. This strategy could also be applied to other polar 2D materials, paving a promising route to prepare wafer-scale polar 2D materials with unique orientation on nonpolar substrates.

Experimental Section

Copper Foil Treatment: The copper foil was first electrochemically polished by phosphoric acid and then rinsed with deionized (DI) water. The polished copper foil was rolled into a tube with a diameter around 3 mm, and then annealed in the chamber at 1035 °C over 2 h under a 25 sccm H_2 flow. The annealed copper tube was unfolded by tweezer and then flattened by being pressed between two glass slides. Finally, this prestressed copper foil was immersed in 10% hydrofluoric acid for 2 min to remove the surface impurities, and then washed by DI water for several cycles just before being loaded into the sealed quartz tube for CVD growth.

Growth of h-BN: The pretreated planar copper foil was loaded into CVD quartz chamber, which was then evacuated down to 0.1 Pa. After flushing the pipeline and chamber with H_2, the H_2 flow rate was fixed at 25 sccm, and then the furnace was heated up to 1035 °C in 50 min and copper foil was annealed once again for 30 min. To grow h-BN, the source (ammonia borane) was heated to 55–80 °C in an isolated quartz container to provide gas precursor which was carried by H_2 into the quartz chamber for the growth of h-BN.[12,13] After the growth, the furnace was cooled down to ambient temperature rapidly.

Characterization: EBSD was performed on JSM-7001F FESEM with collection accessory from EDAX at 20 KV accelerating voltage with the sample stage tilting 70°. TEM and SAED was employed at 200 KV on Tecnai FEI-G^2 F20. XPS was conducted using Al Kα X-ray source.

Density Functional Theory Calculations: The atomic structures, stacking energies and charge densities are calculated in the framework of density functional theory, as implemented in the Vienna Ab Initio Simulation Package (VASP).[33,34] The vdW interactions are considered by using optB88-vdW functional.[35] The cutoff energy is set as 500 eV. The energies and the forces are converged to the accuracy of 1.0×10^{-4} eV and 0.01 eV Å^{-1}, respectively. A vacuum separation of more than 15 Å is adopted in the normal direction (z direction) of Cu surface to prevent interaction between periodic images. The triangular h-BN nucleus is terminated with N atom and the edges are passivated with hydrogen. For each stacking angle, we optimized z coordinate of h-BN nucleus and all the three coordinates x, y, z of Cu atoms of the three top atomic layers.

[1] L. Song, L. Ci, H. Lu, P. B. Sorokin, C. Jin, J. Ni, A. G. Kvashnin, D. G. Kvashnin, J. Lou, B. I. Yakobson, P. M. Ajayan, *Nano Lett.* **2010**, *10*, 3209.

[2] L. H. Li, J. Cervenka, K. Watanabe, T. Taniguchi, Y. Chen, *ACS Nano* **2014**, *8*, 1457.

[3] K. Watanabe, T. Taniguchi, H. Kanda, *Nat. Mater.* **2004**, *3*, 404.

[4] Z. Liu, Y. Gong, W. Zhou, L. Ma, J. Yu, J. C. Idrobo, J. Jung, A. H. MacDonald, R. Vajtai, J. Lou, P. M. Ajayan, *Nat. Commun.* **2013**, *4*, 2541.

[5] C. R. Dean, A. F. Young, I. Meric, C. Lee, L. Wang, S. Sorgenfrei, K. Watanabe, T. Taniguchi, P. Kim, K. L. Shepard, J. Hone, *Nat. Nanotechnol.* **2010**, *5*, 722.

[6] L. Britnell, R. V. Gorbachev, R. Jalil, B. D. Belle, F. Schedin, A. Mishchenko, T. Georgiou, M. I. Katsnelson, L. Eaves, S. V. Morozov, N. M. R. Peres, J. Leist, A. K. Geim, K. S. Novoselov, L. A. Ponomarenko, *Science* **2012**, *335*, 947.

[7] J. Xue, J. Sanchez-Yamagishi, D. Bulmash, P. Jacquod, A. Deshpande, K. Watanabe, T. Taniguchi, P. Jarillo-Herrero, B. J. LeRoy, *Nat. Mater.* **2011**, *10*, 282.

[8] X. Cui, G.-H. Lee, Y. D. Kim, G. Arefe, P. Y. Huang, C.-H. Lee, D. A. Chenet, X. Zhang, L. Wang, F. Ye, F. Pizzocchero, B. S. Jessen, K. Watanabe, T. Taniguchi, D. A. Muller, T. Low, P. Kim, J. Hone, *Nat. Nanotechnol.* **2015**, *10*, 534.

[9] R. V. Gorbachev, A. K. Geim, M. I. Katsnelson, K. S. Novoselov, T. Tudorovskiy, I. V. Grigorieva, A. H. MacDonald, S. V. Morozov, K. Watanabe, T. Taniguchi, L. A. Ponomarenko, *Nat. Phys.* **2012**, *8*, 896.

[10] C. R. Dean, L. Wang, P. Maher, C. Forsythe, F. Ghahari, Y. Gao, J. Katoch, M. Ishigami, P. Moon, M. Koshino, T. Taniguchi, K. Watanabe, K. L. Shepard, J. Hone, P. Kim, *Nature* **2013**, *497*, 598.

[11] C. R. Woods, L. Britnell, A. Eckmann, R. S. Ma, J. C. Lu, H. M. Guo, X. Lin, G. L. Yu, Y. Cao, R. V. Gorbachev, A. V. Kretinin, J. Park, L. A. Ponomarenko, M. I. Katsnelson, Y. N. Gornostyrev, K. Watanabe, T. Taniguchi, C. Casiraghi, H. J. Gao, A. K. Geim, K. S. Novoselov, *Nat. Phys.* **2014**, *10*, 451.

[12] X. Li, J. Yin, J. Zhou, W. Guo, *Nanotechnology* **2014**, *25*, 105701.

[13] J. Yin, J. Yu, X. Li, J. Li, J. Zhou, Z. Zhang, W. Guo, *Small* **2015**, *11*, 4497.

[14] K. K. Kim, A. Hsu, X. Jia, S. M. Kim, Y. Shi, M. Hofmann, D. Nezich, J. F. Rodriguez-Nieva, M. Dresselhaus, T. Palacios, J. Kong, *Nano Lett.* **2012**, *12*, 161.

[15] J. Yin, X. Liu, W. Lu, J. Li, Y. Cao, Y. Li, Y. Xu, X. Li, J. Zhou, C. Jin, W. Guo, *Small* **2015**, *11*, 5375.

[16] F. Müller, K. Stöwe, H. Sachdev, *Chem. Mater.* **2005**, *17*, 3464.

[17] W. Auwärter, H. U. Suter, H. Sachdev, T. Greber, *Chem. Mater.* **2004**, *16*, 343.

[18] Q. Wu, J.-H. Park, S. Park, S. J. Jung, H. Suh, N. Park, W. Wongwiriyapan, S. Lee, Y. H. Lee, Y. J. Song, *Sci. Rep.* **2015**, *5*, 16159.

[19] J.-H. Lee, E. K. Lee, W.-J. Joo, Y. Jang, B.-S. Kim, J. Y. Lim, S.-H. Choi, S. J. Ahn, J. R. Ahn, M.-H. Park, C.-W. Yang, B. L. Choi, S.-W. Hwang, D. Whang, *Science* **2014**, *344*, 286.

[20] V. L. Nguyen, B. G. Shin, D. L. Duong, S. T. Kim, D. Perello, Y. J. Lim, Q. H. Yuan, F. Ding, H. Y. Jeong, H. S. Shin, S. M. Lee, S. H. Chae, Q. A. Vu, S. H. Lee, Y. H. Lee, *Adv. Mater.* **2015**, *27*, 1376.

[21] H. Kroemer, *J. Cryst. Growth* **1987**, *81*, 193.

[22] D. Dumcenco, D. Ovchinnikov, K. Marinov, P. Lazić, M. Gibertini, N. Marzari, O. L. Sanchez, Y.-C. Kung, D. Krasnozhon, M.-W. Chen, S. Bertolazzi, P. Gillet, A. Fontcuberta i Morral, A. Radenovic, A. Kis, *ACS Nano* **2015**, *9*, 4611.

[23] H. Peng, W. Dang, J. Cao, Y. Chen, D. Wu, W. Zheng, H. Li, Z.-X. Shen, Z. Liu, *Nat. Chem.* **2012**, *4*, 281.

[24] F. Orlando, P. Lacovig, L. Omiciuolo, N. G. Apostol, R. Larciprete, A. Baraldi, S. Lizzit, *ACS Nano* **2014**, *8*, 12063.

[25] X. Song, J. Gao, Y. Nie, T. Gao, J. Sun, D. Ma, Q. Li, Y. Chen, C. Jin, A. Bachmatiuk, M. Rümmeli, F. Ding, Y. Zhang, Z. Liu, *Nano Res.* **2015**, *8*, 3164.

[26] E. W. Grace, J. M. Alexander, J. M. James, W. Marc, A. Maria, A. Jose, C. Kai, R. B. Gavin, R. W. Neil, *2D Mater.* **2015**, *2*, 025003.

[27] W. Auwärter, M. Muntwiler, J. Osterwalder, T. Greber, *Surf. Sci.* **2003**, *545*, L735.

[28] C. Jin, F. Lin, K. Suenaga, S. Iijima, *Phys. Rev. Lett.* **2009**, *102*, 195505.

[29] J. Kotakoski, C. H. Jin, O. Lehtinen, K. Suenaga, A. V. Krasheninnikov, *Phys. Rev. B* **2010**, *82*, 113404.

[30] J. Cheng, T. Jiang, Q. Ji, Y. Zhang, Z. Li, Y. Shan, Y. Zhang, X. Gong, W. Liu, S. Wu, *Adv. Mater.* **2015**, *27*, 4069.

[31] Y. Li, Y. Rao, K. F. Mak, Y. You, S. Wang, C. R. Dean, T. F. Heinz, *Nano Lett.* **2013**, *13*, 3329.

[32] J.-M. Zhang, F. Ma, K.-W. Xu, *Appl. Surf. Sci.* **2004**, *229*, 34.

[33] G. Kresse, J. Hafner, *Phys. Rev. B* **1994**, *49*, 14251.

[34] G. Kresse, J. Furthmüller, *Comput. Mater. Sci.* **1996**, *6*, 15.

[35] M. Dion, H. Rydberg, E. Schröder, D. C. Langreth, B. I. Lundqvist, *Phys. Rev. Lett.* **2004**, *92*, 246401.